

# End-to-End Signal Classification in Signed Cumulative Distribution Transform Space

Abu Hasnat Mohammad Rubaiyat, Shiyong Li, Xuwang Yin, Mohammad Shifat-E-Rabbi, Yan Zhuang, and Gustavo K. Rohde

**Abstract**—This paper presents a new end-to-end signal classification method using the signed cumulative distribution transform (SCDT). We adopt a transport-based generative model to define the classification problem. We then make use of mathematical properties of the SCDT to render the problem easier in transform domain, and solve for the class of an unknown sample using a nearest local subspace (NLS) search algorithm in SCDT domain. Experiments show that the proposed method provides high accuracy classification results while being data efficient, robust to out-of-distribution samples, and competitive in terms of computational complexity with respect to the deep learning end-to-end classification methods. The implementation of the proposed method in Python language is integrated as a part of the software package PyTransKit [1].

**Index Terms**—signal classification, time series events, generative model, SCDT, nearest local subspace.

## 1 INTRODUCTION

**S**IGNAL (time series) classification is considered a challenging problem in data science. It refers to the automatic prediction of the class label of a segmented time series event using the information extracted from the corresponding signal intensities. Time series data classification tasks can be found in many applications such as human activity recognition (HAR) [2], physiological signal assessment [3][4], communications [5], structural or machine health monitoring systems [6] [7], financial modeling [8], and others. In many applications (e.g., HAR, ECG, etc.) the time series events of interest can be modeled as instances of a certain (often unknown) template or prototype pattern observed under unknown time warps [9]. Here we propose a new end-to-end tool for classification of signals or time series events of this type using the signed cumulative distribution transform (SCDT), a new mathematical signal transform introduced in [10].

Existing signal classification approaches can be categorized into two broad categories: 1) feature engineering-based classifiers and 2) end-to-end learning classifiers, such as convolutional neural networks (CNNs). Feature engineering-based methods [11] usually rely on the extraction of numerical features (e.g., time domain features, frequency domain features, wavelet features) from the raw signal data, and then the application of different multivariate regression-based classification methods including linear discriminant analysis, support vector machines, random forests, and others. Deep learning-based signal classification methods [12], on the other hand, connect the raw input data to the output class label by utilizing a large number of hidden layers. These methods have widely been studied recently as they have shown high accuracy in certain classification tasks.

Feature engineering signal classification approaches primarily

differ in the types of features chosen to characterize each signal. The bag-of-features framework [13] extracts interval features using fixed- and variable-length intervals, and trains a classifier on the extracted features. Distance-based methods [14] use global (e.g., dynamic time warping (DTW) distance measure [15]) and local (e.g., shapelets [16]) distance features to train the classifier. Ensemble-based approaches such as COTE [17], HIVE-COTE [18], and others combine different features and classifiers to achieve high classification accuracy. All these methods require crafting especially designed features (feature engineering) as well as some amount of data preprocessing.

Approaches based on deep neural networks, especially convolutional neural networks (CNN), have been explored for end-to-end signal classification. Wang et al. [19], for example, provided three standard deep learning benchmark models for end-to-end time series classification: deep multilayer perceptrons (MLP), fully convolutional networks (FCN), and residual networks (ResNet). The method known as multi-scale convolutional neural network (MCNN) [20] is another deep learning approach that takes advantage of CNNs for end-to-end classification of univariate time series. Karim et al. [21] proposed the LSTM-FCN, an improvement over FCN by augmenting the FCN module with a Long Short Term Recurrent Neural Network (LSTM RNN) sub-module. Though they can produce accurate results in many instances, these methods tend to require extensive amounts of training data, are computationally expensive, and often vulnerable to out-of-distribution examples.

In recent years, some effort has been made to exploit transport transforms for signal classification [22] as an alternative to the techniques mentioned above. The cumulative distribution transform (CDT), based on the 1D Wasserstein embedding, was introduced in [23] as a means of classifying strictly positive signals following the linear optimal transport framework proposed in [24]. Aldroubi et al. [10] extended the CDT to general signed signals and proposed the signed cumulative distribution transform (SCDT). Both transforms have a number of properties which allow one to solve nonlinear classification problems using linear classifiers, such as Fisher discriminant analysis, support vector

A. H. M. Rubaiyat, X. Yin, and Y. Zhuang are with the Department of Electrical and Computer Engineering, University of Virginia, Charlottesville, VA 22904 USA (e-mail: {ar3fx, xy4cm, yz8bk}@virginia.edu).

S. Li and M. Shifat-E-Rabbi are with the Department of Biomedical Engineering, University of Virginia, Charlottesville, VA 22908, USA (e-mail: {sl8jx, mr2kz}@virginia.edu).

G. K. Rohde is with the Department of Biomedical Engineering and the Department of Electrical and Computer Engineering, University of Virginia, Charlottesville, VA 22908, USA (e-mail: gustavo@virginia.edu).

TABLE 1: Description of symbols

Symbols	Description
$s(t)$	Signal
$s_0(y)$	Reference signal to calculate the transform
$\widehat{s}(y)/\widehat{s}^\dagger(y)$	SCDT of signal $s$ with/without total mass terms
$g(t)$	Strictly increasing and differentiable function
$s \circ g$	$s(g(t))$ : composition of $s(t)$ with $g(t)$
$\mathcal{T}$	Set of all possible increasing diffeomorphisms
$\mathbb{S}/\widehat{\mathbb{S}}$	Set of signals/SCDT of the signals

machines, or logistic regression, in signal transform space. The classification method proposed in [9] utilizes the nearest subspace method to classify signals in SCDT domain. Assuming the data corresponding to a particular class as compositions of a single template, this method formed a linear subspace for each class. The method we propose here is an extension of this approach.

In this paper, we propose a generic end-to-end technique to classify signals where the signal classes can be modeled as generated from a set of templates under certain time deformations. We represent each data class as a union of subspaces, and employ a nearest local subspace search algorithm in SCDT domain to classify test samples (time series events) that satisfy the generative model described later in this paper. We demonstrate the advantages of the method over alternative end-to-end systems in terms of classification accuracy on a 10 datasets with comprehensive experiments. In addition, experiments highlight other interesting properties of the method in comparison to deep learning solutions including data efficiency, robustness to out-of-distribution conditions, and computational cost.

The remaining of this paper is organized as follows: in section 2, we briefly review the definitions and properties of the CDT and the SCDT. In section 3, we state the classification problem and the proposed solution. Experimental setup, datasets, and results are described in section 4, with the discussion of the results in section 5. Finally, section 6 provides concluding remarks.

## 2 PRELIMINARIES

### 2.1 Notation

Throughout the manuscript, we work with  $L_1$  signals  $s$ , i.e.  $\int_{\Omega_s} |s(t)| dt < \infty$ , where  $\Omega_s \subseteq \mathbb{R}$  is the domain over which  $s$  is defined. We use  $s_{j,m}^{(c)}$  to represent a signal generated from the  $m$ -th template of class  $c$  under deformation  $g_j$ . We denote the  $m$ -th template from class  $c$  as  $\varphi_m^{(c)}$ . Some symbols used throughout the manuscript are listed in Table 1.

### 2.2 The Cumulative Distribution Transform

The Cumulative Distribution Transform (CDT) was introduced in [23] for positive smooth normalized functions. It is an invertible nonlinear 1D signal transform from the space of smooth positive probability densities to the space of diffeomorphisms, which can be described as follows: let  $s(t), t \in \Omega_s$  and  $s_0(y), y \in \Omega_{s_0}$  define a given signal and a reference signal, respectively, such that  $\int_{\Omega_s} s(u) du = \int_{\Omega_{s_0}} s_0(u) du = 1$  and  $s_0(y), s(t) > 0$  in their respective domains. The CDT of the signal  $s(t)$  is then defined to be the function  $s^*(y)$  that solves,

$$\int_{\inf(\Omega_s)}^{s^*(y)} s(u) du = \int_{\inf(\Omega_{s_0})}^y s_0(u) du. \quad (1)$$

Now considering the cumulative distribution functions (CDFs)  $S(t) = \int_{-\infty}^t s(u) du$  and  $S_0(y) = \int_{-\infty}^y s_0(u) du$ , an alternative expression for  $s^*(y)$  is given by,

$$s^*(y) = S^{-1}(S_0(y)). \quad (2)$$

The CDT is therefore seen to inherit the domain of the reference signal. Moreover, if the uniform reference signal is used (i.e.,  $s_0(y) = 1$  in  $\Omega_{s_0} = [0, 1]$ ), we can write  $S_0(y) = y$  and  $s^*(y) = S^{-1}(y)$ . That is to say, the CDT is the inverse of the cumulative distribution function of the given signal  $s(t)$ . Note that the definition of the CDT described above is slightly different from the formulation used in [23]. For simplicity, here we use the CDT definition described in [25]. The CDT is invertible, and the inverse formula is defined in differential form as:

$$s(t) = \left( s^{*-1}(t) \right)' s_0(s^{*-1}(t)). \quad (3)$$

Although the CDT can be used in solving many classification [23] and estimation [25] problems, the framework described above is defined only for positive density functions. Aldroubi et al. [10] extended the CDT to general finite signed signals and named the new signal transformation technique as the signed cumulative distribution transform (SCDT).

### 2.3 The Signed Cumulative Distribution Transform

The signed cumulative distribution transform (SCDT) [10] is an extension of the CDT, which is defined for general finite signed signals with no requirements on the total mass. First, the transform is defined for the non-negative signal  $s(t)$  with arbitrary mass as:

$$\widehat{s}(y) = \begin{cases} (s^*(y), \|s\|_{L_1}), & \text{if } s \neq 0 \\ (0, 0), & \text{if } s = 0, \end{cases} \quad (4)$$

where  $\|s\|_{L_1}$  is the  $L_1$  norm of signal  $s$  and  $s^*$  is the CDT (defined in eqn. (2)) of the normalized signal  $\frac{1}{\|s\|_{L_1}} s$ .

Now for a signed signal, the Jordan decomposition [26] is used to define the transform. The Jordan decomposition of a signed signal  $s(t)$  is given by  $s(t) = s^+(t) - s^-(t)$ , where  $s^+(t)$  and  $s^-(t)$  are the absolute values of the positive and negative parts of the signal  $s(t)$ . The SCDT of  $s(t)$  is then defined as:

$$\widehat{s}(y) = (\widehat{s}^+(y), \widehat{s}^-(y)), \quad (5)$$

where  $\widehat{s}^+(y)$  and  $\widehat{s}^-(y)$  are the transforms (defined in eqn. (4)) for the signals  $s^+(t)$  and  $s^-(t)$ , respectively. Like the CDT, the SCDT is also an invertible operation, with the inverse being,

$$s(t) = \|s^+\|_{L_1} \left( (s^+)^{*-1}(t) \right)' s_0((s^+)^{*-1}(t)) - \|s^-\|_{L_1} \left( (s^-)^{*-1}(t) \right)' s_0((s^-)^{*-1}(t)). \quad (6)$$

Moreover, the SCDT has a number of properties that will help us simplify the signal classification problems.

#### 2.3.1 Composition property

If the SCDT of a signed signal  $s$  is denoted as  $\widehat{s}$ , the SCDT of the signal  $s_g = g' \circ s$  is given by:

$$\widehat{s}_g = (g^{-1} \circ (s^+)^*, \|s^+\|_{L_1}, g^{-1} \circ (s^-)^*, \|s^-\|_{L_1}), \quad (7)$$

where,  $g(t)$  is an invertible and differentiable increasing function,  $s \circ g = s(g(t))$ , and  $g'(t) = dg(t)/dt$  [10]. For example, in case of shift and linear dispersion (i.e.,  $g(t) = \omega t - \tau$ ) of a given signal

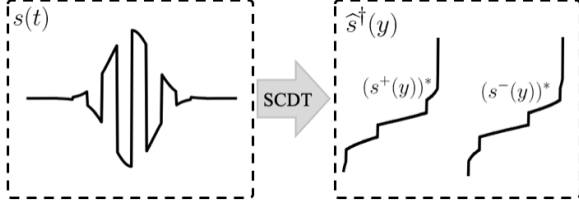


Fig. 1: SCDT (defined in eq. (8)) of an example signal.

$s(t)$ , the SCDT of the signal  $s_g(t) = \omega s(\omega t - \mu)$  can be derived from composition property as:

$$\hat{s}_g = \left( \frac{(s^+)^* + \mu}{\omega}, \|s^+\|_{L_1}, \frac{(s^-)^* + \mu}{\omega}, \|s^-\|_{L_1} \right).$$

The composition property implies that variations along the independent variable caused by  $g(t)$  will change only the dependent variable in the transform domain.

### 2.3.2 Convexity property

Let  $\mathbb{S} = \{s_j | s_j = g'_j \varphi \circ g_j, \forall g_j \in \mathcal{G}\}$  be a set of signals, where  $\varphi$  is a given signal and  $\mathcal{G} \subset \mathcal{T}$  denotes a set of 1D spatial deformations of a specific kind (e.g., translation, dilation, etc.). The convexity property of the SCDT [10] states that the set  $\hat{\mathbb{S}} = \{\hat{s}_j : s_j \in \mathbb{S}\}$  is convex for every  $\varphi$  if and only if  $\mathcal{G}^{-1} = \{g_j^{-1} : g_j \in \mathcal{G}\}$  is convex.

The set  $\mathbb{S}$  defined above can be interpreted as a generative model for a signal class while  $\varphi$  being the template signal corresponding to that class. In the next section we describe a generative model-based problem formulation for time series event classification, and then show how the composition and convexity properties of the SCDT help facilitate signal classification. Note that the SCDT defined above contains the CDTs and the total masses corresponding to the positive and negative parts of the signal. As the signals can be made to have zero mean, the total mass terms (constant scaling factor) will be ignored in this paper, yielding a modified transformed signal:

$$\hat{s}^\dagger(y) = ((s^+(y))^*, (s^-(y))^*). \quad (8)$$

This modified definition of the transformation is used in the proposed solution. Fig. 1 shows an example of the SCDT of a signal calculated using eq. (8).

## 3 PROPOSED METHOD

### 3.1 Generative model and problem statement

In [9], a generative model-based problem statement was proposed for signal classification problems where each signal class can be modeled as instances of a certain template observed under some unknown deformation (e.g., translation, dispersion, etc.). Signal classes of such type can be described with the following generative model:

#### 3.1.1 Generative model (single template)

Let  $\mathcal{G}^{(c)} \subset \mathcal{T}$  denote a set of increasing 1D deformations of a specific kind, where  $\mathcal{T}$  is a set of all possible increasing diffeomorphisms from  $\mathbb{R}$  to  $\mathbb{R}$ . The 1D mass preserving generative model for class  $c$  is then defined to be the set:

$$\mathbb{S}^{(c)} = \{s_j^{(c)} | s_j^{(c)} = g'_j \varphi^{(c)} \circ g_j, g_j \in \mathcal{G}^{(c)}, g'_j > 0\}, \quad (9)$$

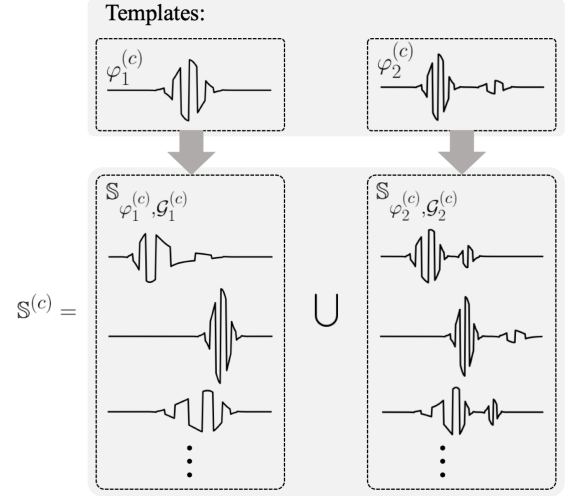


Fig. 2: Generative model example for a signal class ‘c’. The set of all signals from class  $c$  is denoted as  $\mathbb{S}^{(c)}$ , which is modeled as the union of subsets  $\mathbb{S}_{\varphi_m^{(c)}, \mathcal{G}_m^{(c)}}$  (for  $m = 1, 2$ ) containing data generated from a template  $\varphi_m^{(c)}$  under deformation  $\mathcal{G}_m^{(c)}$ .

where  $s_j^{(c)}$  is the  $j$ -th signal from class  $c$ , and  $\varphi^{(c)}$  is the template pattern corresponding to that class. However, in many applications it is difficult to find a signal class that can be represented using the single template-based generative model defined above. In this paper, we use a multiple template-based generative model to represent such signal classes.

#### 3.1.2 Generative model (multiple templates)

For a set of increasing 1D spatial deformations denoted as  $\mathcal{G}^{(c)} \subset \mathcal{T}$ , the 1D mass preserving generative model for class  $c$  is defined to be the set:

$$\begin{aligned} \mathbb{S}^{(c)} &= \bigcup_{m=1}^{M_c} \mathbb{S}_{\varphi_m^{(c)}, \mathcal{G}_m^{(c)}}, \\ \mathbb{S}_{\varphi_m^{(c)}, \mathcal{G}_m^{(c)}} &= \left\{ s_{j,m}^{(c)} | s_{j,m}^{(c)} = g'_j \varphi_m^{(c)} \circ g_j, g'_j > 0, g_j \in \mathcal{G}_m^{(c)} \right\}, \\ \left( \mathcal{G}_m^{(c)} \right)^{-1} &= \left\{ \sum_{i=1}^k \alpha_i f_{i,m}^{(c)}, \alpha_i \geq 0 \right\}, \end{aligned} \quad (10)$$

where  $\{f_{1,m}^{(c)}, f_{2,m}^{(c)}, \dots, f_{k,m}^{(c)}\}$  denotes a set of linearly independent and strictly increasing (within the domain of the signals) functions. Meaning the generative model for class  $c$  is modeled as the union of  $M_c$  subsets, where each subset ( $\mathbb{S}_{\varphi_m^{(c)}, \mathcal{G}_m^{(c)}}$ ) corresponds to data generated from a particular template ( $\varphi_m^{(c)}$ ) under some time deformation ( $\mathcal{G}_m^{(c)}$ ). Here,  $M_c$  is the total number of templates used to represent class  $c$ ,  $\varphi_m^{(c)}$  is the  $m$ -th template signal from class  $c$ , and  $s_{j,m}^{(c)}$  is the  $j$ -th signal generated from  $m$ -th template under deformation defined by  $g_j$ . Fig. 2 illustrates a few examples of such deformations. Considering the generative model, the classification problem can be defined as follows:

**Classification problem:** Let  $\mathcal{G}_m^{(c)} \subset \mathcal{T}$  be a set of spatial deformations and  $\mathbb{S}^{(c)}$  be defined as in eq. (10), for classes  $c = 1, \dots, N_c$ . Given a set of training samples  $\{s_1^{(c)}, s_2^{(c)}, \dots\} \subset \mathbb{S}^{(c)}$  for class  $c$ , determine the class label of an unknown signal  $s$ .

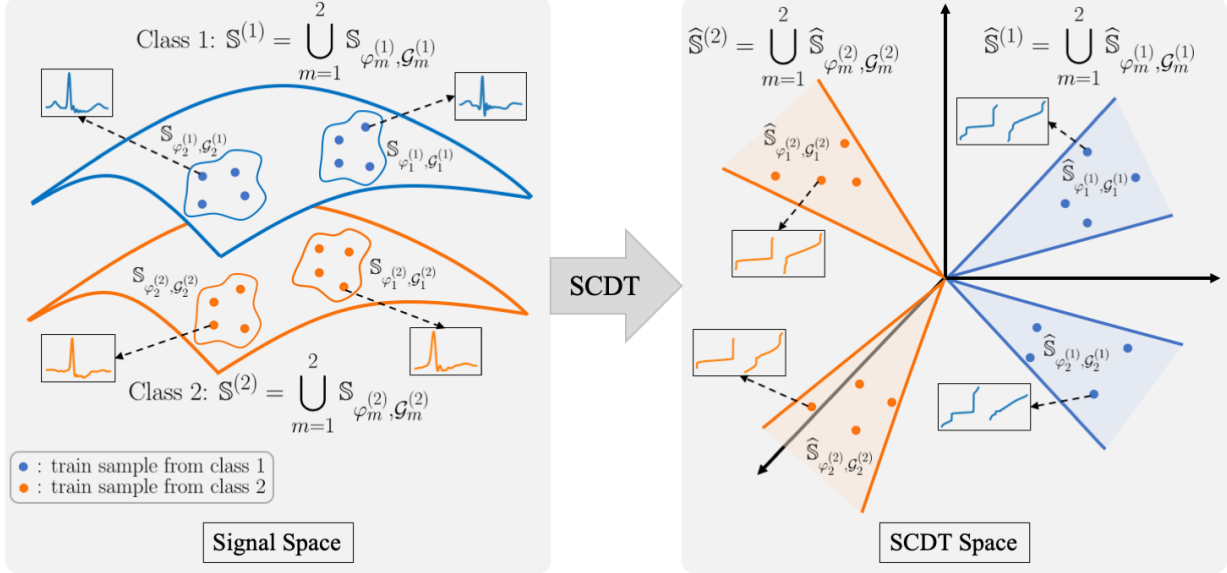


Fig. 3: Geometric interpretation of data following the proposed generative model defined in equations (10) and (11). On the left panel, two classes ( $\mathbb{S}^{(1)}$  and  $\mathbb{S}^{(2)}$ ) are depicted in signal space. The set  $\mathbb{S}^{(c)}$  for class  $c$  is modeled as the union of two subsets:  $\mathbb{S}_{\varphi_1^{(c)}, \mathcal{G}_1^{(c)}}$  and  $\mathbb{S}_{\varphi_2^{(c)}, \mathcal{G}_2^{(c)}}$ ,  $c = 1, 2$ , where both the subsets are non-convex. The right panel shows the geometry of the signal classes in SCDT domain as the union of convex (for convex  $(\mathcal{G}_1^{(c)})^{-1}$  and  $(\mathcal{G}_2^{(c)})^{-1}$  as defined in (10)) subsets:  $\widehat{\mathbb{S}}_{\varphi_1^{(c)}, \mathcal{G}_1^{(c)}}$  and  $\widehat{\mathbb{S}}_{\varphi_2^{(c)}, \mathcal{G}_2^{(c)}}$  for  $c = 1, 2$ .

### 3.2 Proposed solution

We propose a solution to the classification problem defined above using the SCDT in combination with the nearest local subspace method. For a given test sample, the algorithm first searches for  $k$  closest training samples (from a particular class) to the test signal in SCDT domain based on a distance definition specified later. Next, a local subspace is spanned by these samples for each class. The unknown class label of the test sample is then estimated based on the shortest distance from the SCDT of the test signal to these local subspaces.

As stated in [9] and [27], the generative model described in eq. (10) generally yields nonconvex signal classes, causing the above classification problem to be difficult to solve. As specified above in section 2.3.2 (see [10] for more details), under certain assumptions, the geometry of the signal class can be simplified. Hence, the proposed solution begins with applying the SCDT defined in eq. (8) on the input signals. The generative model in the transform domain is then given by,

$$\begin{aligned} \widehat{\mathbb{S}}^{(c)} &= \bigcup_{m=1}^{M_c} \widehat{\mathbb{S}}_{\varphi_m^{(c)}, \mathcal{G}_m^{(c)}}, \\ \widehat{\mathbb{S}}_{\varphi_m^{(c)}, \mathcal{G}_m^{(c)}} &= \left\{ \widehat{s}_{j,m}^{(c)\dagger} \mid \widehat{s}_{j,m}^{(c)\dagger} = g_j^{-1} \circ \widehat{\varphi}_m^{(c)\dagger}, g_j \in \mathcal{G}_m^{(c)} \right\}, \\ \left( \mathcal{G}_m^{(c)} \right)^{-1} &= \left\{ \sum_{i=1}^k \alpha_i f_{i,m}^{(c)}, \alpha_i \geq 0 \right\}, \end{aligned} \quad (11)$$

where  $g_j^{-1} \circ \widehat{\varphi}_m^{(c)\dagger} = \left( g_j^{-1} \circ (\varphi_m^{(c)\dagger})^*, g_j^{-1} \circ (\varphi_m^{(c)-})^* \right)$ . Here, the set  $\left( \mathcal{G}_m^{(c)} \right)^{-1}$  is convex by definition. Therefore, using the convexity property highlighted earlier, it can be shown that  $\widehat{\mathbb{S}}_{\varphi_m^{(c)}, \mathcal{G}_m^{(c)}}$  given in eq. (11) forms a convex set. Moreover, since the SCDT is a one-to-one map, it follows that if  $\mathbb{S}_{\varphi_m^{(c)}, \mathcal{G}_m^{(c)}} \cap \mathbb{S}_{\varphi_w^{(p)}, \mathcal{G}_w^{(p)}} = \emptyset$  for  $c \neq p$ , then  $\widehat{\mathbb{S}}_{\varphi_m^{(c)}, \mathcal{G}_m^{(c)}} \cap \widehat{\mathbb{S}}_{\varphi_w^{(p)}, \mathcal{G}_w^{(p)}} = \emptyset$ . Fig. 3 illustrates

the geometry of signal classes that follow the proposed generative model defined in equations (10) and (11) corresponding to signal and SCDT domains, respectively.

To formulate the solution of the problem defined above, we adapt the subspace-based technique proposed in [9] for the multiple template-based generative model. First, Let us define a subspace generated by the convex set  $\widehat{\mathbb{S}}_{\varphi_m^{(c)}, \mathcal{G}_m^{(c)}}$  as:

$$\widehat{\mathbb{V}}_m^{(c)} = \text{span} \left( \widehat{\mathbb{S}}_{\varphi_m^{(c)}, \mathcal{G}_m^{(c)}} \right). \quad (12)$$

Since  $\widehat{\mathbb{S}}_{\varphi_m^{(c)}, \mathcal{G}_m^{(c)}} \cap \widehat{\mathbb{S}}_{\varphi_w^{(p)}, \mathcal{G}_w^{(p)}} = \emptyset$  (when  $c \neq p$ ) and  $\left( \mathcal{G}_m^{(c)} \right)^{-1}$  is convex by definition, it is reasonable to assume that  $\widehat{\mathbb{S}}^{(c)} \cap \widehat{\mathbb{V}}_w^{(p)} = \emptyset$  for any  $w = 1, \dots, M_p$  (see Appendix A for more explanation). Now, if a test sample  $s$  is generated according to the generative model defined in eq. (10), then there exist a certain class ' $c$ ' and a certain template  $\varphi_m^{(c)}$  for which  $d^2(\widehat{s}^\dagger, \widehat{\mathbb{V}}_m^{(c)}) = 0$ . Here,  $\widehat{s}^\dagger = ((s^+)^*, (s^-)^*)$  is the SCDT of the test sample  $s$ , and  $d^2(\widehat{s}^\dagger, \widehat{\mathbb{V}}_m^{(c)})$  is the Euclidean distance between  $\widehat{s}^\dagger$  and the nearest point in subspace  $\widehat{\mathbb{V}}_m^{(c)}$ . It also follows,  $d^2(\widehat{s}^\dagger, \widehat{\mathbb{V}}_w^{(p)}) > 0$  when  $p \neq c$ . Therefore, under the assumption that the test sample  $s$  is generated according to the generative model for one of the (unknown) classes, the unknown class label can be uniquely predicted by solving,

$$\text{argmin}_c \min_m d^2 \left( \widehat{s}^\dagger, \widehat{\mathbb{V}}_m^{(c)} \right), \quad (13)$$

where  $\widehat{\mathbb{V}}_m^{(c)}$  is given by eq. (12). The proposed algorithm to solve the classification problem is outlined below.

### 3.3 Algorithm: nearest local subspace in SCDT domain

In the signal classification tasks considered below, as usually the case, the template  $\varphi_m^{(c)}$  and the deformation set  $\mathcal{G}_m^{(c)}$  are usually unknown. Therefore the subset  $\widehat{\mathbb{S}}_{\varphi_m^{(c)}, \mathcal{G}_m^{(c)}}$  is also unknown; hence,

we can not readily estimate  $\widehat{\mathbb{V}}_m^{(c)}$  using eq. (12). Here we devise an algorithm to approximate  $\widehat{\mathbb{V}}_m^{(c)}$  using training samples from class  $c$ . Let us assume that the test sample  $s$  is generated according to the generative model  $\mathbb{S}_{\varphi_m^{(c)}, \mathcal{G}_m^{(c)}}$ . From eq. (11),  $\mathbb{S}_{\varphi_m^{(c)}, \mathcal{G}_m^{(c)}}$  can be defined in the SCDT domain as:

$$\widehat{\mathbb{S}}_{\varphi_m^{(c)}, \mathcal{G}_m^{(c)}} = \left\{ \left( \sum_{i=1}^k \alpha_i f_{i,m}^{(c)} \right) \circ \widehat{\varphi}_m^{(c)\dagger}, \alpha_i \geq 0 \right\},$$

where  $\{f_{1,m}^{(c)}, f_{2,m}^{(c)}, \dots, f_{k,m}^{(c)}\}$  is a set of  $k$  linearly independent increasing functions. From this definition, it is evident that  $\widehat{\mathbb{V}}_m^{(c)}$  (as defined in eq. (12)) is a  $k$  dimensional space. Therefore, if we were to estimate this span, we would need at least  $k$  linearly independent elements from the set  $\widehat{\mathbb{S}}_{\varphi_m^{(c)}, \mathcal{G}_m^{(c)}}$  to model it. Since we do not have the knowledge of  $\widehat{\mathbb{S}}_{\varphi_m^{(c)}, \mathcal{G}_m^{(c)}}$ , we employ a nearest local subspace (NLS) search algorithm in SCDT domain to approximate  $\widehat{\mathbb{V}}_m^{(c)}$ . Let us denote the estimated local subspace for class  $c$  as  $\widetilde{\mathbb{V}}_m^{(c)}$ . The solution to the problem defined in eq.(13) is then estimated by solving,

$$\operatorname{argmin}_c d^2 \left( \widehat{s}^\dagger, \widetilde{\mathbb{V}}_m^{(c)} \right). \quad (14)$$

Consider a set of training samples  $\{s_1^{(c)}, \dots, s_j^{(c)}, \dots, s_{L_c}^{(c)}\} \subset \mathbb{S}^{(c)}$  for class  $c$ , where  $L_c$  is the total number of training samples given for class  $c$  and  $s_j^{(c)}$  is the  $j$ -th sample. The unknown class of a test sample  $s$  is estimated in two steps:

**Step 1:** We search for the  $k$  closest training samples to  $\widehat{s}^\dagger$  from class  $c$  based on the distance between  $\widehat{s}^\dagger$  and the span of each training sample. First, we sort the elements from the set  $\{\widehat{s}_1^{(c)\dagger}, \dots, \widehat{s}_{L_c}^{(c)\dagger}\}$  into  $\{\widehat{z}_1^{(c)\dagger}, \dots, \widehat{z}_{L_c}^{(c)\dagger}\}$  such that

$$d^2(\widehat{s}^\dagger, \widehat{\mathbb{V}}_{z_1}^{(c)}) \leq \dots \leq d^2(\widehat{s}^\dagger, \widehat{\mathbb{V}}_{z_l}^{(c)}) \leq \dots, \quad (15)$$

where  $\widehat{\mathbb{V}}_{z_l}^{(c)} = \operatorname{span} \left( \{\widehat{z}_l^{(c)\dagger}\} \right)$ . Then we pick the first  $k$  elements from the sorted set to form  $\{\widehat{z}_1^{(c)\dagger}, \dots, \widehat{z}_k^{(c)\dagger}\}$  for  $k \leq L_c$ , which gives the set of  $k$  closest training samples to  $\widehat{s}^\dagger$  from class  $c$  in the above sense (Fig. 4b-4c). We repeat this step for all other classes (Fig. 4d).

**Step 2:** Compute  $\widetilde{\mathbb{V}}_m^{(c)}$  by:

$$\widetilde{\mathbb{V}}_m^{(c)} = \operatorname{span} \left( \{\widehat{z}_1^{(c)\dagger}, \dots, \widehat{z}_k^{(c)\dagger}\} \right), \quad (16)$$

which approximates the nearest local subspace from class  $c$  with respect to  $\widehat{s}^\dagger$ . We then predict the unknown class of the test sample  $s$  by solving eq. (14). Fig. 4e illustrates the second step. Note that similar local subspace classification techniques can be found in the literature [28] [29]. Here, we employ the nearest local subspace search technique in the SCDT domain to exploit the properties of the SCDT that simplify the classification problem described above. Next, we show that the performance of the classifier can further be improved by utilizing the composition property of the SCDT through analytical enrichment of the subspace method.

### 3.3.1 Subspace enrichment

The algorithm outlined above searches for the  $k$  closest training samples to a given test sample in SCDT domain, and then forms a local subspace using these  $k$  samples. Inspired by [27, 30], here we adapt the technique to mathematically enrich the ensuing subspace with certain prescribed deformations. Here we enrich  $\widetilde{\mathbb{V}}_m^{(c)}$  in such

a way that it will automatically include the samples undergoing certain time-deformations. The spanning sets corresponding to certain specific deformations are derived below:

- **Translation:** In case of translation,  $g(t)$  is given by  $t - \mu$ , where  $\mu \in \mathbb{R}$  is the translation parameter. Using the composition property of the SCDT, the transform of the translated signal  $s_g(t) = s(t - \mu)$  is given by  $\widehat{s}_g^\dagger = ((s^+)^* + \mu, (s^-)^* + \mu)$ . It implies that the translation applied to the signal along the independent axis results in translation along the dependent axis in SCDT domain. Hence, the spanning set for translation is defined as  $\mathbb{U}_T = \{u(t)\}$ , where  $u(t) = 1$ .
- **Dilation:** A time-dilated (scaled) version of a signal  $s(t)$  is defined as:  $s_g(t) = \alpha s(\alpha t)$ ,  $\alpha \in \mathbb{R}^+$ . The transform of the signal  $s_g(t)$  is given by:  $\widehat{s}_g^\dagger = \left( \frac{(s^+)^*}{\alpha}, \frac{(s^-)^*}{\alpha} \right)$ . An additional spanning set is not required for dilation, as it is inherent in the modeling of the subspace.
- **Time-warpings other than translation and dilation** are also observed in certain classification problems. To include those deformations in the SCDT domain, we approximate the increasing function  $g^{-1} \circ \widehat{z}_l^{(c)\dagger}$  as:

$$g^{-1} \circ \widehat{z}_l^{(c)\dagger} = \begin{cases} \sum_{n=-N}^N c_n \zeta_n(\widehat{z}_l^{(c)\dagger}) & \text{for } n \neq 0 \\ c_0 \widehat{z}_l^{(c)\dagger} & \text{for } n = 0 \end{cases} \quad (17)$$

where,  $c_n > 0$ ,  $\sum_{n=-N}^N c_n = 1$ , and

$$\zeta_n(\widehat{z}_l^{(c)\dagger}) = \left[ \widehat{z}_l^{(c)\dagger} - \frac{\sin n\pi \widehat{z}_l^{(c)\dagger}}{|n|\pi} \right].$$

For the set  $\{\widehat{z}_1^{(c)\dagger}, \dots, \widehat{z}_k^{(c)\dagger}\}$  from eq. (16), the spanning set is given by the set  $\mathbb{U}_H = \{\zeta_n(\widehat{z}_1^{(c)\dagger}), \dots, \zeta_n(\widehat{z}_k^{(c)\dagger})\}$ , for  $n = -N, \dots, -1, 1, \dots, N$ .

In light of the discussion above, the subspace  $\widetilde{\mathbb{V}}_m^{(c)}$  in eq. (16) can be enriched as follows:

$$\widetilde{\mathbb{V}}_m^{(c)} = \operatorname{span} \left( \{\widehat{z}_1^{(c)\dagger}, \dots, \widehat{z}_k^{(c)\dagger}\} \cup \mathbb{U}_T \cup \mathbb{U}_H \right). \quad (18)$$

Note that the subspace  $\widehat{\mathbb{V}}_{z_l}^{(c)}$  in (15) can also be enriched in similar manner, i.e.  $\widehat{\mathbb{V}}_{z_l}^{(c)} = \operatorname{span} \left( \{\widehat{z}_l^{(c)\dagger}\} \cup \mathbb{U}_T \cup \mathbb{U}_H \right)$ , where  $\mathbb{U}_H = \{\zeta_n(\widehat{z}_l^{(c)\dagger})\}$ , for  $n = -N, \dots, -1, 1, \dots, N$ .

### 3.3.2 Training phase

In the training phase of the algorithm, the subspace corresponding to each of training sample is calculated. The first step is to compute SCDTs for all training samples from class  $c$ . Then, we take a training sample  $\widehat{s}_l^{(c)\dagger}$  and orthogonalize  $\{\widehat{s}_l^{(c)\dagger}\} \cup \mathbb{U}_T \cup \mathbb{U}_H$  to obtain the basis vectors that span the enriched subspace corresponding to that sample. Let  $B_l^{(c)} = [b_{l,1}^{(c)}, b_{l,2}^{(c)}, \dots]$  be a matrix that contains the basis vectors in its column. We repeat these calculations for all the training samples to form  $B_l^{(c)}$  for  $l = 1, 2, \dots, L_c$  and  $c = 1, 2, \dots$ , etc.

### 3.3.3 Testing phase

The testing algorithm begins with taking SCDT of the test sample  $s$  to obtain  $\widehat{s}^\dagger$  followed by the nearest local subspace search in SCDT domain. In the first step of the algorithm, we estimate the

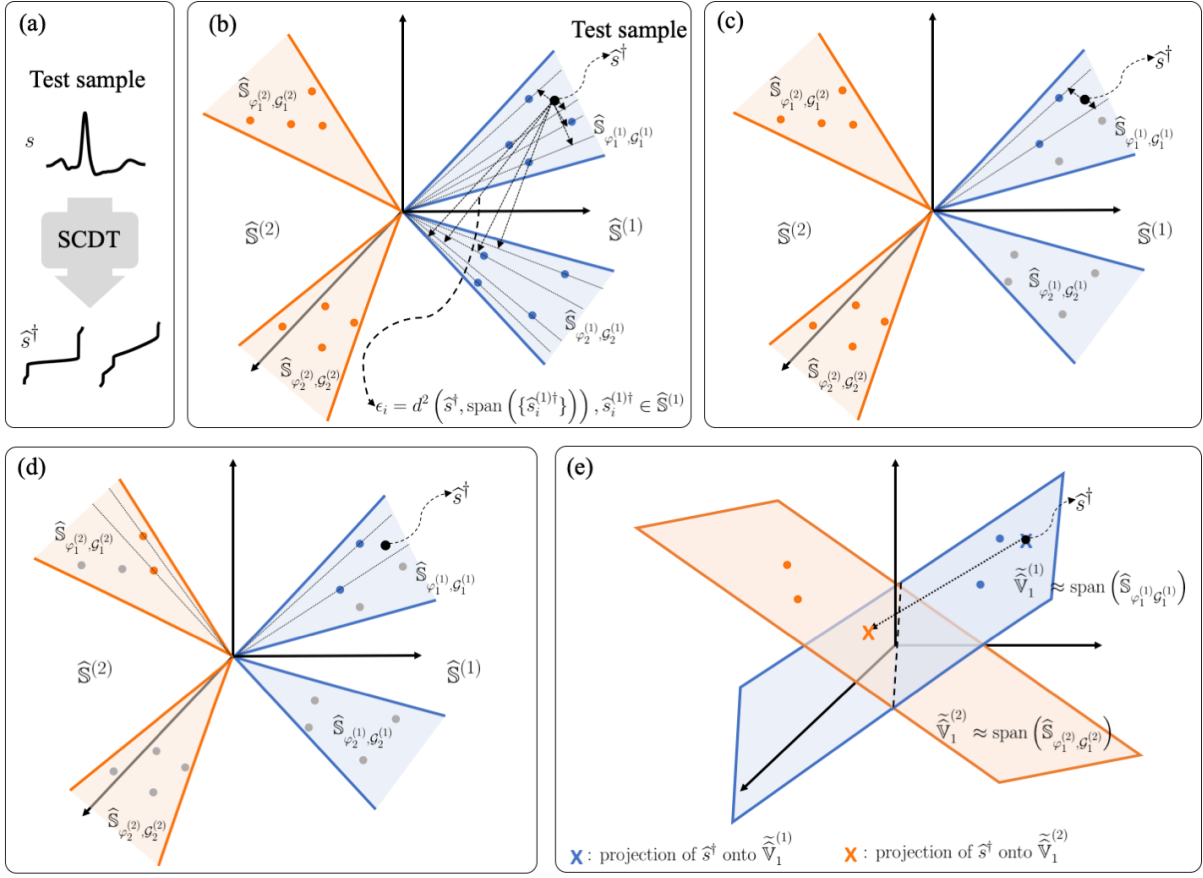


Fig. 4: Outline of proposed algorithm: (a) apply SCDT on the test signal  $s$  to obtain  $\hat{s}^\dagger$ , (b) measure distance between  $\hat{s}^\dagger$  and subspace corresponding to each training sample from a particular class (class-1 in this example), (c) find  $k$  closest training samples ( $k = 2$  in this example) to  $\hat{s}^\dagger$  from class-1, (d) repeat previous steps for other classes (class-2 in this example), (e) build local subspace for each class using the  $k$  samples found in previous steps and search for the nearest local subspace to predict the class of  $s$ .

distance of the subspace corresponding to each of the training samples from  $\hat{s}^\dagger$  by:

$$\epsilon_l = \|\hat{s}^\dagger - B_l^{(c)} B_l^{(c)T} \hat{s}^\dagger\|^2, \quad l = 1, 2, \dots, L_c,$$

where  $\|\cdot\|$  denotes  $L_2$  norm. Note that  $B_l^{(c)} B_l^{(c)T}$  is the orthogonal projection matrix onto the space generated by the span of the columns of  $B_l^{(c)}$  (computed in the training phase). We then find  $\{\hat{z}_1^{(c)\dagger}, \dots, \hat{z}_k^{(c)\dagger}\}$ , a set of  $k$  closest training samples to the test sample  $\hat{s}^\dagger$  from class  $c$ , based on the distances  $\epsilon_1, \dots, \epsilon_{L_c}$ . In the next step, we orthogonalize  $\{\hat{z}_1^{(c)\dagger}, \dots, \hat{z}_k^{(c)\dagger}\} \cup U_T \cup U_H$  to obtain the basis vectors  $\{b_1^{(c)}, b_2^{(c)}, \dots\}$  spanning the local subspace from class  $c$  with respect to  $\hat{s}^\dagger$ . Let  $B^{(c)} = [b_1^{(c)}, b_2^{(c)}, \dots]$  for  $c = 1, 2, \dots, s$  etc. The unknown class of  $s$  is then estimated by:

$$\arg \min_c \|\hat{s}^\dagger - B^{(c)} B^{(c)T} \hat{s}^\dagger\|. \quad (19)$$

Note that the proposed algorithm requires two parameters  $k$  and  $N$  (see eq. (17)) to be tuned prior to the testing phase. We use a validation set split from the training set to estimate the optimum values for these parameters. We then follow the steps of the proposed algorithm outlined above with the validation set for varying  $k$  and  $N$ . Parameter values corresponding to the best validation accuracy are chosen to be used in the testing phase. This step is done during the training phase.

### 3.4 Proof-of-concept simulation

To demonstrate the efficacy of the proposed algorithm in solving the classification problem stated in section 3.1 we performed a simulated experiment. We took six prototype signals shown in Fig. 5 as the templates ( $\varphi_m^{(c)}$ ) corresponding to three different classes ( $c = 1, 2, 3$ ), i.e., each class has two templates ( $m = 1, 2$ ). We then generated a synthetic dataset by applying specific time deformations on the prototype signals as follows:

$$\begin{aligned} s_j^{(c)} &= g_j'(t) \varphi_m^{(c)}(g_j(t)), \\ g_j(t) &= \omega \zeta(t) + \tau, \quad g_j'(t) > 0, \\ \zeta'(t) &= \frac{\partial}{\partial t} \zeta(t) = \sum_{n=1}^N \alpha_n \frac{1}{\sqrt{2\pi} w_n} e^{-\frac{1}{2} \left( \frac{t - \mu_n}{w_n} \right)^2}, \\ \sum_n \alpha_n &= 1, \quad \alpha_n > 0 \end{aligned} \quad (20)$$

where the parameter values used to calculate  $g_j(t)$  are randomly chosen from fixed intervals. The dataset was equally split into training and testing sets. The proposed classification method was then trained with a varying number of training samples per class randomly chosen from the training set and evaluated on the testing set. Note that the samples were chosen in such a way that the training set contains an equal number of samples generated from each template. The test accuracy plot in Fig. 5 with respect to

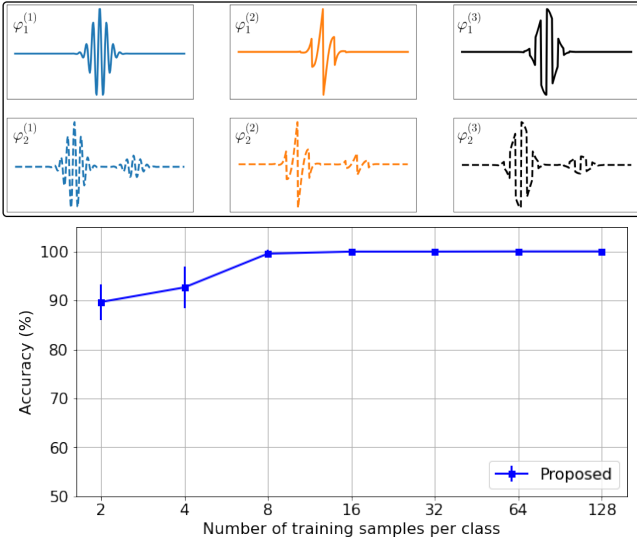


Fig. 5: A simulated experiment to demonstrate the efficacy of the proposed method in classifying signal classes that follow the generative model defined in eq. (10).

the number of training samples per class shows that the proposed method achieves the perfect classification accuracy with few training samples (obtained 100% test accuracy with only 16 training samples per class) if the signal classes follow the generative model defined in eq. (10).

## 4 EXPERIMENTS AND RESULTS

### 4.1 Experimental setup

The goal is to evaluate the performance of the proposed generic end-to-end classifier with respect to selected state-of-the-art CNN-based time series classification techniques. The classification performance of the different methods were studied in terms of test accuracy, data efficiency, computational efficiency, and robustness to the out-of-distribution samples. We conducted experiments on several time series data and compared the results against several methods: Multilayer Perceptrons (MLP) [31], 1D Visual Geometry Group (VGG) [31], 1D Residual Network (ResNet) [32] [31], Long Short Term Memory (LSTM) [33] [31], and Long Short Term Memory Fully Convolutional Network (LSTM-FCN) [21] [31]. For the neural network methods, we used the implementations outlined in [31] without any data augmentation. During the training process, 10% of the training samples were used as the validation set, and the test performance was reported based on the model that had the best validation performance. To show the efficacy of the proposed multiple template-based generative model (defined in eq. (10)) over the single template-based model (defined in eq. (9)), we also compared the results against the SCDT-NS classifier [9] proposed earlier.

We followed the training and testing procedures outlined in the previous section for the proposed method. The orthogonalization operations were performed using singular value decomposition (SVD). The left singular vectors obtained by the SVDs were used to construct the matrices  $B_l^{(c)}$  and  $B^{(c)}$ . Following [27], the number of the basis vectors was chosen in such a way that the sum of variances explained by the selected basis vectors captures at least 99% of the total variance explained by all the samples in the sorted set  $\{\hat{z}_1^{(c)\dagger}, \dots, \hat{z}_k^{(c)\dagger}\}$ . The SCDTs were computed with respect to a 1D uniform probability density function.

### 4.2 Datasets

To evaluate the comparative performance of the proposed method with respect to deep learning-based end-to-end classifiers we selected multiple datasets with signal classes representing well-defined time series events. For example, the accelerometer data plotted in Fig. 6(a) represent particular hand gestures. Similarly, signals shown in Fig. 6(j) represent either normal or abnormal heartbeats. With a focus towards this condition, we identified ten different time series datasets, nine of which were downloaded from the UCR time series classification archive [34]. The remaining dataset is a well-known ECG dataset collected from the PhysioNet MIT-BIH Arrhythmia database [35]. Some example signals from these datasets are shown in Fig. 6. Note that all the signals are pre-processed to have zero mean. Details about the datasets are given below:

- *GesturePebbleZ2* [36]: Accelerometer data collected using Pebble smart watch from 4 different persons performing 6 hand gestures. (classes: 6, train samples: 22 ~ 25 per class, test samples: 25 ~ 32 per class).
- *InsectEPGRegularTrain* [37]: Contains electrical penetration graph (EPG) data which capture voltage changes of the electrical circuit that connects insects and their food source. (classes: 2, train samples: 22 ~ 30 per class, test samples: 89 ~ 118 per class).
- *Trace*: A subset of the Transient Classification Benchmark (Trace project) [38]. It is a synthetic dataset designed to simulate instrumentation failures in a nuclear power plant. (classes: 4, train samples: 21 ~ 31 per class, test samples: 19 ~ 24 per class).
- *PLAID*: Plug Load Appliance Identification Dataset [39]. The data are intended for load identification research using transient voltage/current measurements from 11 different appliance types. (classes: 11, train samples: 13 ~ 88 per class, test samples: 13 ~ 87 per class).
- *UWaveGestureLibraryAll* [40]: A set of eight simple gestures generated from accelerometers using Wii remote. (classes: 8, train samples: 100 ~ 127 per class, test samples: 433 ~ 460 per class).
- *Wafer* [41]: A collection of inline process control measurements recorded from various sensors during the processing of silicon wafers. The two classes are normal and abnormal, with a significant class imbalance. Hence, a subset of the original dataset is used to ensure the class balance. (classes: 2, train samples: 97 ~ 100 per class, test samples: 665 ~ 700 per class).
- *StarLightCurves* [42]: Collection of time series signals representing the brightness of celestial objects as a function of time. (classes: 3, train samples: 150 per class, test samples: 500 per class).
- *TwoPatterns* [43]: A simulated dataset (classes: 4, train samples: 237 ~ 271 per class, test samples: 959 ~ 1035 per class).
- *ECG5000* [34]: A subset of BIDMC Congestive Heart Failure Database (CHFDB) downloaded from PhysioNet. With a purpose of evaluating the methods trained with a large set, we interchanged the train and test sets of the original dataset. (classes: 2, train samples: 1873 ~ 2627 per class, test samples: 208 ~ 292 per class).
- *MITBIH-AAMI* [35]: A subset of MIT-BIH Arrhythmia database collected from PhysioNet. Two classes (normal

beats and premature ventricular contraction) with the highest number of samples were used. (classes: 2, train samples: 1200 per class, test samples: 1000 per class).

In addition to the datasets listed above, we have used another dataset where time series events are not well-defined as an example where the proposed method is not expected to work well. We have used the gearbox fault diagnosis data [44], a collection of vibration signals recorded by using SpectraQuest’s Gearbox Fault Diagnostics Simulator. The dataset was recorded in two different scenarios: 1) healthy and 2) broken tooth conditions.

### 4.3 Test accuracy

To demonstrate the efficacy of the proposed method as a generic classifier, we applied it to the datasets listed above and compared the test accuracies against the aforementioned deep learning-based methods. Table 2 shows the results and a comprehensive comparison with five other end-to-end neural network-based classifiers. We also compared the results against the SCDT-NS classifier [9] to demonstrate the advantages of the method proposed here. The results reported in the table show that the proposed method achieved best test accuracies for 8 out of 10 datasets, while the closest method is the 1D-VGG model which achieved the best results in 2 cases. The average arithmetic and geometric ranking also support the claim that the proposed method is the best generic end-to-end technique to classify segmentable time series events.

Besides test accuracy and rank-based statistics, we also calculated mean per class error (MPCE) [19] for each method. MPCE is defined as the arithmetic mean of the per class error (PCE) which is calculated for  $i$ -th model on  $j$ -th dataset as:  $PCE_{i,j} = \frac{e_{i,j}}{c_j}$ . Here  $e_{i,j}$  is the error rate of  $i$ -th model on  $j$ -th dataset, and  $c_j$  is the total number of classes present in  $j$ -th dataset. MPCE for the corresponding model is given by,

$$MPCE_i = \frac{1}{J} \sum_{j=1}^J PCE_{i,j},$$

where  $J$  is the total number of datasets used in the experiment. The MPCE values reported in Table 2 indicate that the proposed method generates the least expected error rate per class across all the datasets with respect to other classifiers.

### 4.4 Data efficiency

To show the data efficiency of the proposed method, we set up an experiment where we trained the models with a varying number of training samples per class. For a training split of a particular size, its samples were randomly drawn from the original training set, and the experiments for this particular size were repeated 10 times. Fig. 7 shows average accuracies with respect to the number of training samples per class for two datasets: *UWaveGestureLibraryAll* and *TwoPatterns*. The standard deviation for each split is also shown using the error bar. The plots illustrate that the proposed method achieves higher accuracy than the other methods with fewer training samples. Similar results can be seen in other datasets as well (see Appendix B).

### 4.5 Robust to out-of-distribution samples

To demonstrate the robustness to out-of-distribution examples, we adopted a similar concept used in [9]. We generated a synthetic dataset by applying time deformations defined in eq. (20) on three

prototype signals: a Gabor wave, an apodized sawtooth wave, and an apodized square wave (shown in the top row of Fig. 7). Note that we used a single template per class to generate data for maintaining a simple experimental setup. We varied the magnitude of the confounding factors (i.e., the parameters used to calculate  $g_j(t)$ ) to generate different distributions for training and testing sets. The ‘in-distribution’ set used during the training process consisted of signals with parameter values chosen randomly from smaller intervals with respect to the ‘out-distribution’ (testing) set. Table 3 shows the list of the parameters of interest for the ‘out-of-distribution’ experiment. The intervals (from which the parameter values were chosen) corresponding to the training and testing sets are also given in the table. Fig. 8 shows test accuracies with respect to the number of training samples per class for the comparing methods. The plot shows that the proposed method significantly outperforms the neural networks with very few training samples. Meaning, the proposed classification technique provides the best classification result if the test signal belongs to the ‘out-distribution’ set in the above sense but follows the generative model discussed in the previous section.

### 4.6 Computational efficiency

Fig. 9 plots the number of floating point operations (FLOPS) required during the training phase as a function of accuracy for each method with the datasets *UWaveGestureLibraryAll* and *TwoPatterns*. Note that the training phase of the proposed method includes an exhaustive grid search technique for tuning the parameters  $k$  and  $N$ . Although this step requires a significant amount of computations, the proposed method still provides competitive performance in terms of computational efficiency in comparison with deep learning-based methods. Fig. 9 shows that only MLP provided  $\sim 90\%$  accuracy on the *UWaveGestureLibraryAll* dataset with fewer computations than the proposed method, whereas the proposed method is  $\sim 1000$  times more efficient than the other methods in achieving  $\sim 90\%$  accuracy on the *TwoPatterns* dataset.

### 4.7 A dataset that does not follow generative model

As described in 4.2, the proposed method performs well if the time series data is well segmented, i.e. contains events with well defined start and end points. There are examples of signal classification problems where data do not follow these conditions. One such example is the gearbox fault diagnosis dataset [44], where vibration signals are used to detect a faulty gearbox. Fig. 10(a) shows that the vibration signals do not possess segmentable time series events. Hence, the proposed method is not suitable for classifying raw gearbox vibration data, as shown in the table in Fig. 10. However, we can transform each time series to frequency domain using the Fourier transform [45], where signals of finite length are necessarily band limited (and thus have a beginning and end in frequency domain). As expected the proposed method performs better when applied to the frequency domain signals shown in Fig. 10(b).

## 5 DISCUSSION

Classification test accuracies, rank-based statistics, and MPCE reported in Table 2 across 10 different time series datasets suggest that the proposed method is the best generic end-to-end signal classification model for time series containing segmented events.



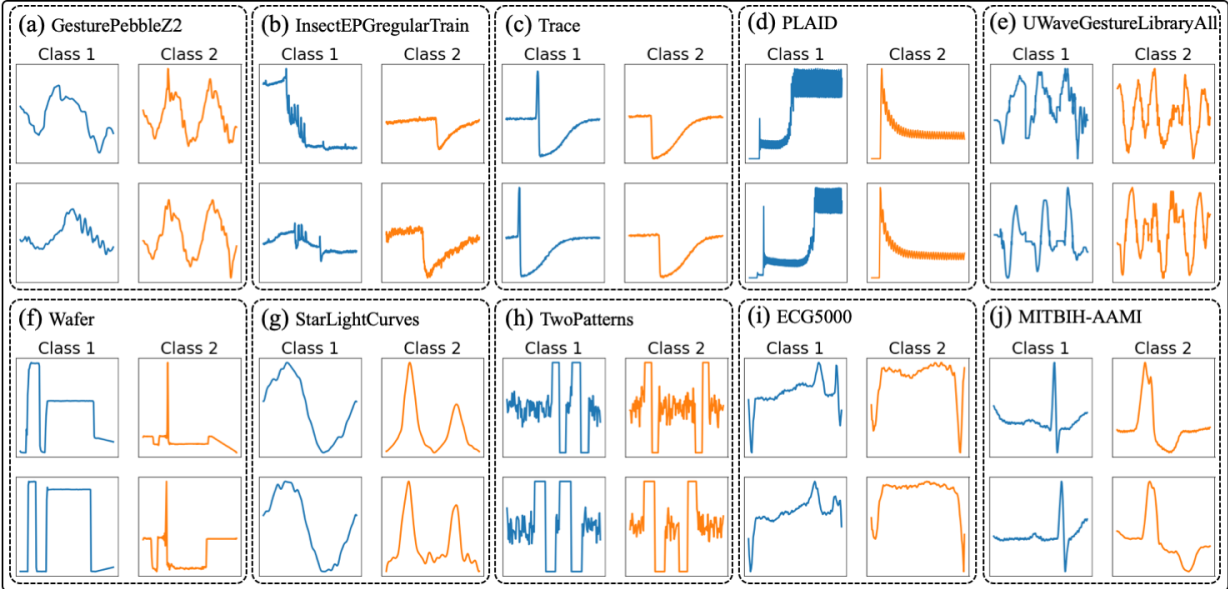


Fig. 6: Example signals from the ten datasets used to evaluate the proposed method.

Dataset	MLP	1D-VGG	1D-ResNet	LSTM	LSTM-FCN	SCDT-NS	<b>Proposed</b>
GesturePebbleZ2	83.92	48.99	63.23	60.19	85.82	81.64	<b>86.07</b>
InsectEPGRegularTrain	80.92	82.07	50.58	57.05	59.95	73.43	<b>90.82</b>
Trace	64.0	35.8	25.9	28.2	58.1	85.0	<b>88.0</b>
PLAID	39.65	19.35	29.81	26.35	39.57	58.29	<b>70.02</b>
UWaveGestureLibraryAll	94.74	<b>96.42</b>	42.86	30.72	94.16	90.4	94.92
Wafer	68.69	94.03	53.66	51.36	86.70	92.75	<b>95.53</b>
StarLightCurves	75.85	70.0	56.53	60.54	74.38	77.4	<b>84.2</b>
TwoPatterns	88.12	95.15	87.42	80.62	98.47	95.15	<b>99.92</b>
ECG5000	98.9	<b>98.92</b>	<b>98.92</b>	98.36	98.76	93.4	97.4
MITBIH-AAMI	65.54	82.94	59.13	55.34	79.46	62.9	<b>84.05</b>
Win	0	2	1	0	0	0	<b>8</b>
AVG arithmetic ranking	3.5	3.5	5.6	6.3	3.6	3.8	<b>1.6</b>
AVG geometric ranking	3.42	2.8	5.07	6.27	3.46	3.49	<b>1.28</b>
MPCE	0.072	0.065	0.125	0.127	0.066	0.059	<b>0.030</b>

TABLE 2: Test accuracy (%), rank-based statistics, and MPCE calculated for the classifiers across ten different datasets.

Parameter	Train	Test
$N$	[2, 5]	[2, 10]
$\mu_n$	$\mathcal{N}(0.5, 0.2)$	$\mathcal{N}(0.5, 0.3)$
$\omega$	[0.9, 1.1]	[0.75, 1.25]
$\tau$	[-0.05, 0.05]	[-0.1, 0.1]

TABLE 3: Intervals used in the out-of-distribution setup.

Moreover, Fig. 7 shows that the proposed method can achieve higher accuracy than the deep learning-based classifiers with fewer training samples. The computational efficiency of the proposed classifier is also demonstrated in Fig. 9 in terms of the GFLOPs count required by the different models during the training phase to achieve a particular test accuracy. It is also evident from Table 2 that the proposed method outperforms the SCDT-NS classifier [9] which uses a single template-based generative model.

Another compelling property of the proposed method is the robustness to the out-of-distribution samples, meaning, it generalizes to samples outside the known distribution when the signal classes conform to the specific generative model. Plots in Fig. 8 show that the performance of CNN-based methods drastically fall under the out-of-distribution setup, whereas the proposed method

achieves perfect test accuracy with very few training samples ( $\sim 16$  per class). The reason behind the robustness to the out-of-distribution setup is that the proposed method is capable of learning the underlying data model, more specifically, the types of deformations present in the signals. It can then successfully classify an unknown signal in presence of such deformations but with different magnitudes.

The main assumption of the proposed method is that the dataset needs to conform to the underlying generative model proposed earlier. Specifically, we showed above that the method works best when the time series (signal) being classified contains segmented events with finite duration. Fig. 10 shows an example where raw signals (from a gearbox vibration experimental setup) do not possess well-defined time series events of finite duration. Hence, the proposed method performs poorly in classifying those signals. However, the same signals in frequency domain seem to fit the generative model better and the proposed method performs better in classifying the gearbox data in frequency domain.

## 6 CONCLUSION

This paper introduced a new end-to-end signal classification method based on a recently developed signal transform. First, we

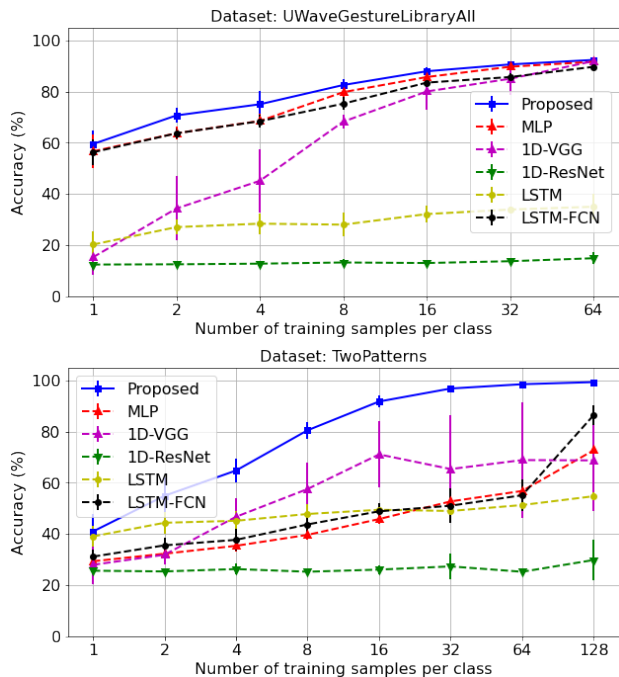


Fig. 7: Accuracy as a function of number of training samples per class for different classification methods.

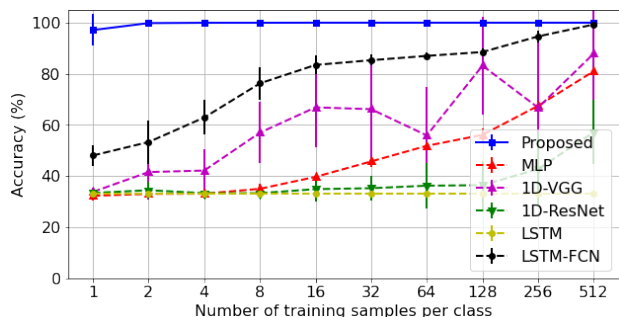


Fig. 8: Accuracy as a function of number of training samples per class under the out-of-distribution setup.

formulated the problem statement based on a multiple template-based generative model observed under unknown deformations. Then, we proposed an end-to-end solution to the problem by employing a nearest local subspace search algorithm in SCDD domain. Although the problem statement and solution are based on the assumption that signals are observation of templates under confounding deformations, knowledge of these templates or confound deformations is not required. The model was demonstrated to achieve high test accuracy across multiple time series datasets. Several experiments show that the proposed method not only outperforms the state-of-the-art deep learning based end-to-end methods but also is data efficient and robust to out-of-distribution examples. Moreover, it shows competitive performance with respect to the CNNs in terms of computational complexity. We note that the approach assumes that the data being classified follows a certain generative model. Namely, each time series should contain an event with finite support, that is, with beginning and end within the recorded time series. We showed that for signal classes that do not contain events of finite length the approach is less effective. Future work will include exploring ways to extend this method to classify time series events that are not readily segmentable.

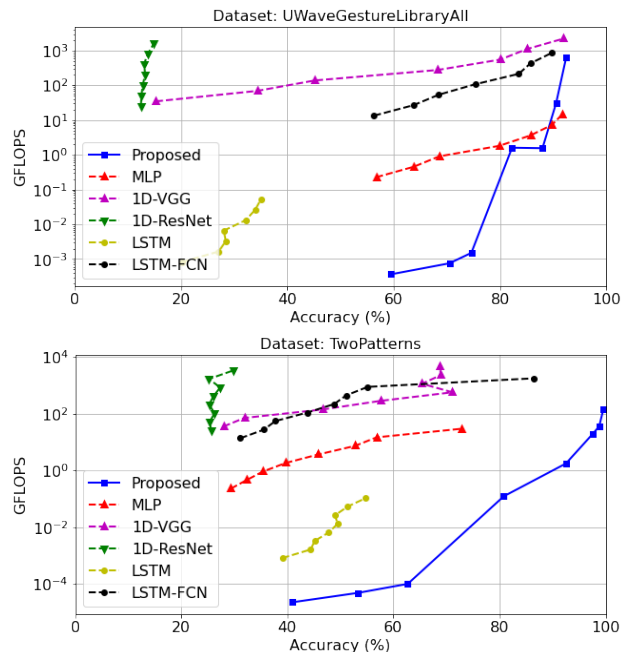
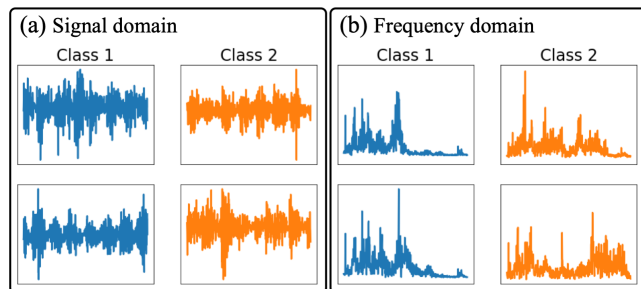


Fig. 9: Giga-floating point operations (GFLOPs) count as a function of test accuracy for different classification methods.



Method	Time domain	Frequency domain
MLP	60.67	67.47
1D-VGG	50.77	55.57
1D-ResNet	79.82	70.88
LSTM	61.22	68.64
LSTM-FCN	<b>80.83</b>	<b>88.47</b>
SCDD-NS	53.1	78.0
<b>Proposed</b>	62.30	87.20

Fig. 10: Plots in (a) show few examples from the gearbox fault diagnosis dataset that do not follow the generative model. Plots in (b) show the signals in frequency domain corresponding to the signals shown in (a), which seem to fit the generative model; hence, the proposed method performs better in classifying these signals. Table in lower panel shows the test accuracy (%) generated by the classifiers on both time and frequency domain data.

## APPENDIX A ADDITIONAL FACTS AND REMARKS

Observation 1: Let  $c \neq p$  be two class labels, and  $\mathbb{S}^{(c)}$  and  $\mathbb{S}^{(p)}$  be defined as in eq. (10), respectively. Assume that for any  $\varphi_j^{(c)} \in \mathbb{S}^{(c)}$ ,  $f_{j, \varphi_w^{(p)}} \notin \text{span}\{(\mathcal{G}_w^{(p)})^{-1}\}$  for any  $w = 1, \dots, M_p$  where  $(f_{j, \varphi_w^{(p)}})' \varphi_j^{(c)} (f_{j, \varphi_w^{(p)}}) = \varphi_w^{(p)}$ , it follows that  $\widehat{\mathbb{V}}_w^{(p)} \cap \widehat{\mathbb{S}}^{(c)} = \emptyset$  for any  $w = 1, \dots, M_p$ .

Proof. Assume by contradiction that there exists some  $\varphi_j^{(c)} \in \mathbb{S}^{(c)}$  such that  $\widehat{\varphi}_j^{(c)} \in \widehat{\mathbb{V}}_w^{(p)} \cap \widehat{\mathbb{S}}^{(c)}$ . By the composition property and the definition of  $f_{j,\varphi_w^{(p)}}$  above, we have that  $f_{j,\varphi_w^{(p)}}^{-1} \circ \widehat{\varphi}_j^{(c)} = \widehat{\varphi}_w^{(p)}$  and hence  $\widehat{\varphi}_j^{(c)} = f_{j,\varphi_w^{(p)}} \circ \widehat{\varphi}_w^{(p)}$ . Since by assumption  $\widehat{\varphi}_j^{(c)} \in \widehat{\mathbb{V}}_w^{(p)}$ , it follows that  $f_{j,\varphi_w^{(p)}} \in \text{span}\left\{(\mathcal{G}_w^{(p)})^{-1}\right\}$ , which is a contradiction.

Remark 1: The last argument above follows from the simple fact that  $\widehat{\mathbb{V}}_w^{(p)} = \text{span}\left(\widehat{\mathbb{S}}_{\varphi_w, \mathcal{G}_w^{(p)}}\right) = \left\{\sum_{i=1}^k \beta_i f_{i,w}^{(p)} \circ \widehat{\varphi}_w^{(p)} : \beta_i \in \mathbb{R}\right\} = \left\{f \circ \widehat{\varphi}_w^{(p)} : f \in \text{span}(\mathcal{G}_w^{(p)})^{-1}\right\}$ .

Remark 2: By the disjointness assumption about different signal classes, i.e.,  $\mathbb{S}^{(p)} \cap \mathbb{S}^{(c)} = \emptyset$  for  $c \neq p$ , it follows that  $f_{j,\varphi_w^{(p)}} \notin (\mathcal{G}_w^{(p)})^{-1}$  for all  $p = 1, \dots, M_p$ . This property intuitively says that signals in  $\mathbb{S}^{(c)}$  differs “significantly” from the template  $\varphi_w^{(p)}$  in the sense that they can not be recovered using  $\varphi_w^{(p)}$  under deformations in  $\mathcal{G}_w^{(p)}$ . Recall that  $(\mathcal{G}_w^{(p)})^{-1} = \left\{\sum_{i=1}^k \alpha_i f_{i,w}^{(p)} : \alpha_i \geq 0\right\}$ ,

which differs from  $\text{span}\left\{(\mathcal{G}_w^{(p)})^{-1}\right\}$  in the sense that the latter has no restriction on the  $\alpha_i$ ’s. We comment loosely that the assumptions in Observation 1 is not unreasonable when signals in class  $(c)$  are ”significantly” different than templates in class  $(p)$  and the deformation sets are reasonably “small” in the sense that  $f_{j,\varphi_w^{(p)}} \notin \text{span}\left\{(\mathcal{G}_w^{(p)})^{-1}\right\}$ .

## APPENDIX B

### DATA EFFICIENCY OF THE PROPOSED METHOD

Section IV-D of the paper shows that the proposed method is data efficient in comparison with the CNNs and provides two examples. Fig. 11 shows the results from same experiment setup for eighth other datasets.

### ACKNOWLEDGEMENTS

This work was supported in part by NIH grant GM130825.

### REFERENCES

- [1] Imaging and data science lab, “PyTransKit,” <https://github.com/rohdelab/PyTransKit>.
- [2] O. D. Lara and M. A. Labrador, “A survey on human activity recognition using wearable sensors,” *IEEE communications surveys & tutorials*, vol. 15, no. 3, pp. 1192–1209, 2012.
- [3] S. K. Berkaya, A. K. Uysal, E. S. Gunal, S. Ergin, Serkan G., and M. B. Gulmezoglu, “A survey on ECG analysis,” *Biomedical Signal Processing and Control*, vol. 43, pp. 216–235, 2018.
- [4] A. Subasi and M. I. Gursoy, “EEG signal classification using PCA, ICA, LDA and support vector machines,” *Expert systems with applications*, vol. 37, no. 12, pp. 8659–8666, 2010.
- [5] A. Fehske, J. Gaeddert, and Jeffrey H. Reed, “A new approach to signal classification using spectral correlation and neural networks,” in *First IEEE International Symposium on New Frontiers in Dynamic Spectrum Access Networks, 2005. DySPAN 2005*. IEEE, 2005, pp. 144–150.
- [6] Osama Abdeljaber, Onur Avci, Mustafa Serkan Kiranyaz, Boualem Boashash, Henry Sodano, and Daniel J Inman, “1-D CNNs for structural damage detection: Verification on a structural health monitoring benchmark data,” *Neurocomputing*, vol. 275, pp. 1308–1317, 2018.
- [7] R. Zhao, R. Yan, Z. Chen, K. Mao, P. Wang, and R. X. Gao, “Deep learning and its applications to machine health monitoring,” *Mechanical Systems and Signal Processing*, vol. 115, pp. 213–237, 2019.
- [8] C. Lu, T. Lee, and C. Chiu, “Financial time series forecasting using independent component analysis and support vector regression,” *Decision support systems*, vol. 47, no. 2, pp. 115–125, 2009.
- [9] Abu Hasnat Mohammad Rubaiyat, Yan Zhuang, Shiyang Li, Gustavo K Rohde, et al., “Nearest subspace search in the signed cumulative distribution transform space for 1D signal classification,” *arXiv preprint arXiv:2110.05606*, 2021.
- [10] A. Aldroubi, R. D. Martin, I. Medri, G. K. Rohde, and S. Thareja, “The signed cumulative distribution transform for 1-D signal analysis and classification,” *Foundations of Data Science*, 2022.
- [11] Anthony Bagnall, Jason Lines, Aaron Bostrom, James Large, and Eamonn Keogh, “The great time series classification bake off: a review and experimental evaluation of recent algorithmic advances,” *Data mining and knowledge discovery*, vol. 31, no. 3, pp. 606–660, 2017.
- [12] Hassan Ismail Fawaz, Germain Forestier, Jonathan Weber, Lhassane Idoumghar, and Pierre-Alain Muller, “Deep learning for time series classification: a review,” *Data mining and knowledge discovery*, vol. 33, no. 4, pp. 917–963, 2019.
- [13] Mustafa Gokce Baydogan, George Runger, and Eugene Tuv, “A bag-of-features framework to classify time series,” *IEEE transactions on pattern analysis and machine intelligence*, vol. 35, no. 11, pp. 2796–2802, 2013.
- [14] Amaia Abanda, Usue Mori, and Jose A Lozano, “A review on distance based time series classification,” *Data Mining and Knowledge Discovery*, vol. 33, no. 2, pp. 378–412, 2019.
- [15] Steinn Gudmundsson, Thomas Philip Runarsson, and Sven Sigurdsson, “Support vector machines and dynamic time warping for time series,” in *2008 IEEE International Joint Conference on Neural Networks (IEEE World Congress on Computational Intelligence)*. IEEE, 2008, pp. 2772–2776.
- [16] Lexiang Ye and Eamonn Keogh, “Time series shapelets: a new primitive for data mining,” in *Proceedings of the 15th ACM SIGKDD international conference on Knowledge discovery and data mining*, 2009, pp. 947–956.
- [17] Anthony Bagnall, Jason Lines, Jon Hills, and Aaron Bostrom, “Time-series classification with COTE: the collective of transformation-based ensembles,” *IEEE Transactions on Knowledge and Data Engineering*, vol. 27, no. 9, pp. 2522–2535, 2015.
- [18] Jason Lines, Sarah Taylor, and Anthony Bagnall, “Time series classification with HIVE-COTE: The hierarchical vote collective of transformation-based ensembles,” *ACM Transactions on Knowledge Discovery from Data*, vol. 12, no. 5, 2018.
- [19] Zhiguang Wang, Weizhong Yan, and Tim Oates, “Time series classification from scratch with deep neural networks: A strong baseline,” in *2017 International joint conference on neural networks (IJCNN)*. IEEE, 2017, pp. 1578–1585.
- [20] Zhicheng Cui, Wenlin Chen, and Yixin Chen, “Multi-scale

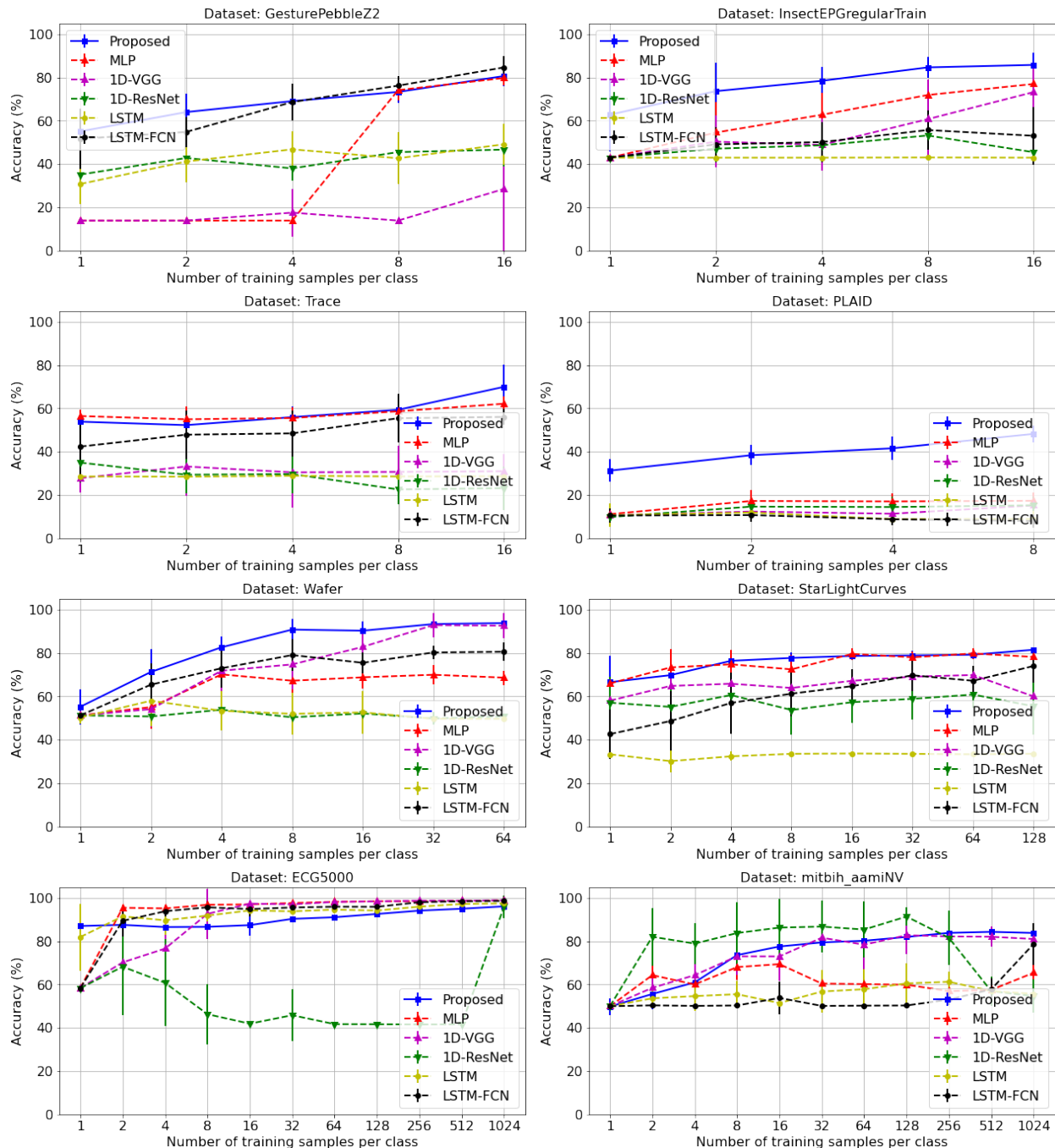


Fig. 11: Accuracy as a function of number of training samples per class for different classification methods.

convolutional neural networks for time series classification,” *arXiv preprint arXiv:1603.06995*, 2016.

- [21] Fazle Karim, Somshubra Majumdar, Houshang Darabi, and Shun Chen, “LSTM fully convolutional networks for time series classification,” *IEEE access*, vol. 6, pp. 1662–1669, 2017.
- [22] S. Kolouri, S. R. Park, M. Thorpe, D. Slepcev, and G. K Rohde, “Optimal mass transport: Signal processing and machine-learning applications,” *IEEE signal processing magazine*, vol. 34, no. 4, pp. 43–59, 2017.
- [23] S. R. Park, S. Kolouri, S. Kundu, and G. K. Rohde, “The cumulative distribution transform and linear pattern recognition,” *Applied and computational harmonic analysis*, vol.

45, pp. 616–641, 2018.

- [24] W. Wang, D. Slepcev, S. Basu, J. A Ozolek, and G. K Rohde, “A linear optimal transportation framework for quantifying and visualizing variations in sets of images,” *International journal of computer vision*, vol. 101, no. 2, pp. 254–269, 2013.
- [25] A. H. M. Rubaiyat, K. M. Hallam, J. M. Nichols, M. N. Hutchinson, S. Li, and G. K. Rohde, “Parametric signal estimation using the cumulative distribution transform,” *IEEE Transactions on Signal Processing*, vol. 68, pp. 3312–3324, 2020.
- [26] H. L. Royden and P. Fitzpatrick, *Real analysis*, vol. 32, Macmillan New York, 1988.

- [27] M. Shifat-E-Rabbi, X. Yin, A. H. M. Rubaiyat, S. Li, S. Kolouri, A. Aldroubi, J. M. Nichols, and G. K. Rohde, "Radon cumulative distribution transform subspace modeling for image classification," *Journal of Mathematical Imaging and Vision*, pp. 1–19, 2021.
- [28] Jorma Laaksonen, "Local subspace classifier," in *International Conference on Artificial Neural Networks*. Springer, 1997, pp. 637–642.
- [29] Hakan Cevikalp, Diane Larlus, Matthijs Douze, and Frédéric Jurie, "Local subspace classifiers: Linear and nonlinear approaches," in *2007 IEEE Workshop on Machine Learning for Signal Processing*. IEEE, 2007, pp. 57–62.
- [30] Mohammad Shifat E Rabbi, Yan Zhuang, Shiyang Li, Abu Hasnat Mohammad Rubaiyat, Xuwang Yin, and Gustavo K Rohde, "Invariance encoding in sliced-Wasserstein space for image classification with limited training data," *arXiv preprint arXiv:2201.02980*, 2022.
- [31] Brian Kenji Iwana and Seiichi Uchida, "An empirical survey of data augmentation for time series classification with neural networks," *Plos one*, vol. 16, no. 7, pp. e0254841, 2021.
- [32] Hassan Ismail Fawaz, Germain Forestier, Jonathan Weber, Lhassane Idoumghar, and Pierre-Alain Muller, "Data augmentation using synthetic data for time series classification with deep residual networks," *arXiv preprint arXiv:1808.02455*, 2018.
- [33] Sepp Hochreiter and Jürgen Schmidhuber, "Long short-term memory," *Neural computation*, vol. 9, no. 8, pp. 1735–1780, 1997.
- [34] Hoang Anh Dau, Eamonn Keogh, Kaveh Kamgar, Chia Michael Yeh, Yan Zhu, Shaghayegh Gharghabi, Chotirat Ann Ratanamahatana, Yanping, Bing Hu, Nurjahan Begum, Anthony Bagnall, Abdullah Mueen, Gustavo Batista, and Hexagon-ML, "The UCR time series classification archive," October 2018, [https://www.cs.ucr.edu/~eamonn/time\\_series\\_data\\_2018/](https://www.cs.ucr.edu/~eamonn/time_series_data_2018/).
- [35] Sajad Mousavi and Fatemeh Afghah, "Inter-and intra-patient ECG heartbeat classification for arrhythmia detection: a sequence to sequence deep learning approach," in *ICASSP 2019-2019 IEEE International Conference on Acoustics, Speech and Signal Processing (ICASSP)*. IEEE, 2019, pp. 1308–1312.
- [36] Antigoni Mezari and Ilias Maglogiannis, "Gesture recognition using symbolic aggregate approximation and dynamic time warping on motion data," in *Proceedings of the 11th EAI International Conference on Pervasive Computing Technologies for Healthcare*, 2017, pp. 342–347.
- [37] Denis S Willett, Justin George, Nora S Willett, Lukasz L Stelinski, and Stephen L Lapointe, "Machine learning for characterization of insect vector feeding," *PLoS computational biology*, vol. 12, no. 11, pp. e1005158, 2016.
- [38] Davide Roverso, "Multivariate temporal classification by windowed wavelet decomposition and recurrent neural networks," in *3rd ANS international topical meeting on nuclear plant instrumentation, control and human-machine interface*. Citeseer, 2000, vol. 20.
- [39] Jingkun Gao, Suman Giri, Emre Can Kara, and Mario Bergés, "PLAID: a public dataset of high-resolution electrical appliance measurements for load identification research: demo abstract," in *proceedings of the 1st ACM Conference on Embedded Systems for Energy-Efficient Buildings*, 2014, pp. 198–199.
- [40] Jiayang Liu, Lin Zhong, Jehan Wickramasuriya, and Venu Vasudevan, "uWave: Accelerometer-based personalized gesture recognition and its applications," *Pervasive and Mobile Computing*, vol. 5, no. 6, pp. 657–675, 2009.
- [41] Robert Thomas Olszewski, *Generalized feature extraction for structural pattern recognition in time-series data*, Carnegie Mellon University, 2001.
- [42] Umaa Rebbapragada, Pavlos Protopapas, Carla E Brodley, and Charles Alcock, "Finding anomalous periodic time series," *Machine learning*, vol. 74, no. 3, pp. 281–313, 2009.
- [43] Pierre Geurts, *Contributions to decision tree induction: bias/variance tradeoff and time series classification*, Ph.D. thesis, ULiège-University of Liège, 2002.
- [44] National Renewable Energy Laboratory, "Gearbox fault diagnosis data [data set]," 2018, <http://data.openei.org/submissions/623>.
- [45] Ronald Newbold Bracewell and Ronald N Bracewell, *The Fourier transform and its applications*, vol. 31999, McGraw-hill New York, 1986.